Research in Astron. Astrophys. **2013** Vol. **13** No. **11**, 1381–1396
http://www.raa-journal.org *http://www.iop.org/journals/raa*

Research in Astronomy and Astrophysics

Onboard GRB trigger algorithms of SVOM-GRM *

Dong-Hua Zhao[1,2], Bo-Bing Wu[1], Li-Ming Song[1], Yong-Wei Dong[1], Stéphane Schanne[3], Bertrand Cordier[3] and Jiang-Tao Liu[1]

[1] Institute of High Energy Physics, Chinese Academy of Sciences, Beijing 100049, China; *zhaodh@ihep.ac.cn*
[2] National Astronomical Observatories, Chinese Academy of Sciences, Beijing 100012, China
[3] CEA Saclay, DSM/Irfu/Service d'Astrophysique, 91191, Gif-sur-Yvette, France

Received 2012 August 14; accepted 2013 June 14

Abstract The Gamma-Ray Monitor (GRM) is a high energy detector onboard the future Chinese-French satellite named the Space-based multi-band astronomical Variable Object Monitor which is dedicated to studies of gamma-ray bursts (GRBs). This paper presents an investigation of the algorithms that look for GRBs by searching for a significant increase in the photon count rate for the computer onboard GRM. The trigger threshold and trigger efficiency, which are based on a given sample of GRBs, are calculated with the algorithms. The trigger characteristics of onboard instruments GRM and ECLAIRs are also analyzed. In addition, the impact of solar flares on GRM is estimated, and a method to distinguish solar flares from GRBs is investigated.

Key words: trigger algorithms — gamma-rays: bursts — Sun: flares

1 INTRODUCTION

Gamma-ray bursts (GRBs), which are flashes of gamma-rays associated with extremely energetic explosions at cosmological distances, are short and unpredictable. The bandwidths of satellite telemetry are not large enough to send every detection event to the ground in real time. In addition, the satellite will encounter many non-GRB events during the monitoring process which can introduce false triggers into the detector. These factors demonstrate the importance of developing onboard trigger algorithms for the following three purposes: (1) to detect GRBs as early as possible which makes it possible to detect the early afterglow and to allow follow-up observations of the GRBs with high redshift; (2) to increase the trigger efficiency of GRBs and the types of GRBs; (3) to decrease the false trigger rate, and to identify the false trigger. A common and easily understood trigger algorithm, which searches for count increases over small timescales and estimates the backgrounds by taking an average of the count rate from a period before the burst, has been employed by most previous observing missions in this field (Vela, PVO, ISEE-3, Ginga and BATSE). In such a trigger algorithm, a large threshold ($\geq 11\sigma$) was usually set to decrease the number of false triggers. However, even with such a large threshold, most of the results still had a high false trigger rate. The statistical fluctuations and the trends in the background are the two main factors causing false triggers, and the latter one becomes a critical factor when using a large threshold. In addition to the traditional trigger algorithm, the High Energy Transient Explorer-2 (HETE-2) (Fenimore & Galassi 2001; Tavenner

* Supported by the National Natural Science Foundation of China.

et al. 2003) estimates the background in the region where the trigger is being sampled by fitting a polynomial to counts from regions considered to be the background. Such trigger algorithms can effectively remove the trends in the background and allow HETE-2 to use a much smaller threshold than previous observing missions. The Burst Alert Telescope (BAT) onboard *Swift* (Fenimore et al. 2003, 2004; McLean et al. 2004) has also adopted similar trigger algorithms.

The Space-based multi-band astronomical Variable Object Monitor (SVOM) is a LEO mission with an altitude of 600 km and an inclination of 30°. Like *Swift*, SVOM (Paul et al. 2011; Basa et al. 2008) can rapidly slew the low energy instruments (MXT and VT) to the sources for follow-up observations. Before starting this operation, the satellite needs to confirm that there is a burst localized by the high energy detectors which are the Gamma-Ray Monitor (GRM) and ECLAIRs. Both GRM and ECLAIRs can acquire trigger information by the counting rate trigger algorithm, and ECLAIRs can further confirm the source and obtain its location by the image trigger algorithm (Schanne et al. 2008).

GRM is sensitive in the energy range from $\sim$30 keV to $\sim$5 MeV. It is a phoswich detector which consists of three scintillating layers consisting of a plastic scintillator, NaI(Tl) and CsI(Na). The three kinds of scintillators, with a combined diameter of 190 mm, are glued together and attached to the same light guide that is coupled to a photomultiplier tube. The thicknesses of the plastic scintillator, NaI(Tl) and CsI(Na) are respectively 6, 15, and 35 mm. NaI(Tl) works as the main detection element of GRM while CsI(Na) is another important detection element and also serves as an anti-coincidence element against photons coming from behind. The plastic scintillator is dedicated to rejecting the background events that are due to charged particles with low energy. The beryllium plate with a thickness of 1.5 mm is chosen as an entrance window for this triple phoswich detector. The collimator that is made of tantalum is located in front of the scintillator case to reduce the background by limiting the field of view (FOV) to 2.5 sr. ECLAIRs is a coded-mask imaging camera for X- and gamma-rays with a 2 sr FOV and a 1024 cm^2 detector area. It mainly consists of a detection plane of 80×80 CdTe semiconductor detectors, a coded-mask located above the detection plane, a multi-layer lateral shield between the detection plane and the mask, and some mechanical structures. Its range of energy for detection is 4–250 keV. We have built a model of GRM and ECLAIRs with the Geant4 package. For the detailed descriptions of the instruments, see the references (Zhao et al. 2012; Dong et al. 2009; Godet et al. 2009; Mandrou et al. 2008).

In this study, we investigate the onboard GRB trigger algorithms of GRM in detail based on the given GRB sample and estimate the impact of solar flares on GRM. The paper is organized as follows. The GRB sample used in developing the trigger algorithms is briefly described in Section 2. We study three counting rate trigger algorithms, try to find the most sensitive energy ranges and timescales, and compare the trigger characteristics of GRM and ECLAIRs in Section 3. In order to search for the method to reject false triggers, we analyze the impact of solar flares on GRM and investigate how to distinguish the triggers caused by solar flares from those by GRBs in Section 4. Finally, in Section 5, we conclude with a concise summary and a discussion of some limitations in this work as well as some further studies that are required.

2 THE GRB SAMPLE

We collect a sample of GRBs consisting of 249 long GRBs and 103 short ones for testing the trigger algorithms. All of the spectra we used are time-integrated spectra.

The spectra of long GRBs are from table 9 in Kaneko et al. (2006). These GRBs are selected from 2704 GRBs observed by BATSE based on the criterion of a peak photon flux in 256 ms (50–300 keV) being greater than 10 photon s^{-1} cm^{-2} or a total energy fluence in the summed energy range ($\sim$20–2000 keV) being larger than 2.0×10^{-5} erg cm^{-2}. A set of photon models were used to fit each GRB in the energy range 30–2000 keV, and the best-fit model was chosen according to χ^2

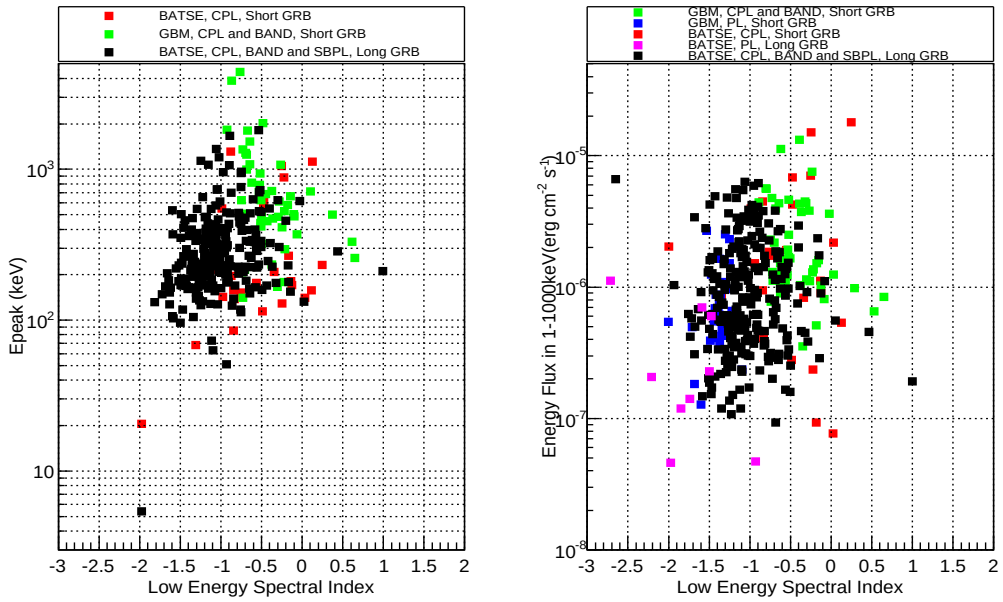

Fig. 1 The distribution of the GRB sample on the plot of low energy spectral index vs. $E_{\rm peak}$ and on the plot of low energy spectral index vs. energy flux.

probabilities and parameter constraints. Excluding those GRBs which have no information[1] on their duration or no data on flux/fluence, we get 249 long GRBs.

For 103 short GRBs, 26 GRBs are from BATSE (Ghirlanda et al. 2004) and the other 77 short GRBs are from GBM (Nava et al. 2011). In Ghirlanda et al. (2004), the authors selected the short GRBs (T_{90} $\leq$2 s) with a peak flux (computed on a timescale of 64 ms and integrated over energy range 50–300 keV) exceeding 10 photon cm^{-2} s^{-1} from the GRB catalog[2] and fitted them with the Comptonization model (Ghirlanda et al. 2002) in the energy range $\sim$30 keV–1.8 MeV. A sample of 28 short GRBs with 100–300 keV fluence $\geq 2.4 \times 10^{-7}$ erg cm^{-2} was obtained. Excluding the two GRBs with uncertain $E_{\rm peak}$, we finally get 26 short GRBs. In Nava et al. (2011), the spectra of GRBs detected by GBM up to March 2010 were analyzed with the single power-law model, Band function and Comptonization model, which are defined in Kaneko et al. (2006). 77 short GRBs with the best-fit model were obtained.

The parameter distributions of the GRB sample are shown in Figure 1. The spectra of short GRBs with the average low energy spectral index of –0.72 are harder than those of long GRBs with index of –1.07. The average $E_{\rm peak}$ of short GRBs (excluding the GRBs with spectra of PL) is 662 keV, which is larger than that of long GRBs (294 keV). The average energy flux (2.3×10^{-6} erg cm^{-2} s^{-1}) of short GRBs is approximately two times that of long GRBs (1.2×10^{-6} erg cm^{-2} s^{-1}).

The long and short GRBs described above are bright GRBs with relatively high peak photon flux and energy fluence. In addition, we select another set of GRBs, which we call dark GRBs hereafter, by reducing the flux of the bright GRBs and keeping other features the same. Thus, we get a GRB sample including bright and dark GRBs to test the trigger algorithms of GRM. All of the

[1] *http://gammaray.msfc.nasa.gov/batse/grb/catalog/current/tables/duration_table.txt*

[2] *http://cossc.gsfc.nasa.gov/cossc/batse/*

light curves required are from the dataset of BATSE[3]. For the GRBs detected by GBM, we select the corresponding light curve of BATSE with a similar duration.

We get the detected spectra of GRBs by inputting the corresponding spectra into the model built with Geant4. Then we can get the time information for each detected photon by random sampling according to the corresponding light curves. Finally, we can obtain the detected photon lists with energy and time information which will be used as the input data to investigate the trigger algorithms of GRM and ECALIRs.

3 THE GRB TRIGGERS

In this section, we study the GRB triggers for GRM with the trigger algorithms that compute the counting rate. We describe three kinds of these counting rate trigger algorithms, and compute the corresponding trigger threshold and trigger efficiency. We also analyze the GRB triggers of ECLAIRs in the same way for comparisons. NaI(Tl) is the main detection crystal in GRM and the threshold and efficiency of GRM discussed in this section are applicable to this device configuration which we will denote as GRM_NaI. Other corresponding device configurations will be denoted similarly.

3.1 Counting Rate Trigger Algorithms

The counting rate trigger algorithm is a method to look for GRBs by searching for a "significant" increase in the photon count rate over a background count rate. The photon count rate generally corresponds to a given energy range, timescale and region in the detector plane. The region in the detector plane is applicable to the pixel detector but not to the scintillation detector like GRM. For the preliminary studies of the GRB trigger of ECLAIRs, we do not consider the region in the detector plane. Triggering in different energy ranges can be used to adjust the detector sensitivity to hard or soft GRBs, while triggering on different timescales can make the detector sensitive to long or short GRBs. We select 30–50, 50–150, 150–300, 300–550 and 550–5000 keV as the trigger energy ranges for GRM and select 4–50, 4–80, 4–120 and 15–50 keV for ECLAIRs considering the detection efficiency and the spectral features of GRBs. One of the important reasons why the energy range is finely divided is that we will try to reject false triggers by analyzing the distribution of triggers in different energy ranges, which is discussed in Section 4. In addition, we need to prepare for the simultaneous operations of both GRM and ECLAIRs for being GRB triggers. According to the experience from the previous satellites, we adopt $5\,\mathrm{ms}\times 2^n$ as the trigger timescales for GRM and ECLAIRs. We define 5–80 ms as short timescales and 160 ms–40 s as long timescales.

Generally, in the trigger algorithm, the time when there is no apparent emission from a GRB is called the background period (hereafter called Back) and that when the GRB will probably produce strong emissions is the foreground period (hereafter called Fore) (Fenimore et al. 2003). The algorithms operating on short and long timescales are called the short rate trigger algorithm and long rate trigger algorithm, respectively. In the short rate trigger algorithm, the background during Fore is expressed by the average count rate in Back during a period before Fore occurs (Fenimore & Galassi 2001; Tavenner et al. 2003). Such an algorithm is very appropriate for short GRB triggers in real time because it is computationally simple and fast. In the long rate trigger algorithm on long timescales, the period needed to compute the background is much longer during which the trend of the background is obvious. In order to deal with this trend, generally people will fit the background with a proper function. A simple and effective linear function is used in our studies. Then we can effectively subtract the background during the Fore by interpolating or extrapolating the fitting function. The long rate trigger in which all of the Backs are before the Fore is called a long one-sided trigger, and that in which some Backs are after the Fore is called a long bracketed trigger. We denote the Backs before and after the Fore by Back1 and Back2, respectively. The long bracketed trigger

[3] *http://www.hep.csdb.cn/browsall/compton/data/batse/ascii_data/64ms/*

can be used to subtract the background during the Fore most accurately, but it needs the longest time because the trigger has to be delayed until after Back2. In order to reduce the delay time, Back2 is usually much shorter than Back1 and the space between Back2 and Fore is also shorter. The parameter setting of the trigger algorithm is discussed in Tavenner et al. (2003). In order to detect all kinds of GRBs in real time and measure the spectra as completely as possible, we can simultaneously run these three kinds of trigger algorithms on the onboard computers.

3.2 Trigger Threshold

With the three kinds of trigger algorithms described above, we investigate the GRB triggers of GRM and ECLAIRs. In Zhao et al. (2012), we simulated the background of GRM and ECLAIRs for seven typical positions of Earth relative to the FOV. With the same method and the given relative position of Earth on the orbit, we can understand how the background varies with the orbit of the satellite with respect to time. In this study, we only consider one factor in this process, namely the position of Earth. For ECLAIRs, we take into account three kinds of gamma-ray backgrounds. For GRM, we also consider the delayed background caused by the trapped high energy protons in SAA to be approximately a constant, because it will not obviously change with respect to the relative position of Earth. From the background simulations, we know that ECLAIRs has more background counts than GRM in their own energy ranges, and the background of ECLAIRs varies with respect to the position of Earth more obviously than that of GRM.

With the background, we can set the threshold which should cause neither too many false triggers nor too low of a trigger efficiency. There are 70 (56) combinations of trigger energy range and timescale for GRM (ECLAIRs). For each combination, we compute the threshold in the way inspired by the method in McLean et al. (2004). Firstly, we study how the background, varying with the satellite orbit, corresponds to different combinations. Then, we run the trigger algorithms with no injected bursts under the background conditions to compute the corresponding maximum value $S_{\max}$=(Fore–Back)/$\sqrt{\mathrm{Back}}$ for each combination. Finally, we set the appropriate threshold according to $S_{\max}$. In order to avoid false triggers due to the known background, we set $S_{\max}$+0.5 as the threshold in this study. The thresholds of GRM and ECLAIRs with different trigger algorithms in various energy ranges and on different timescales are shown in Figure 2. The data from GRM and ECLAIRs are denoted by solid triangles and solid dots, respectively. The data due to different trigger algorithms are indicated by different colors. In the top panel, different values for each timescale correspond to different energy ranges. In the bottom two panels, the different values for each energy range correspond to different timescales. In order to analyze how the threshold changes with the energy ranges, we use the upper limit to express the corresponding trigger energy range (one exception: 15 keV for ECLAIRs expresses the energy range 15–50 keV). The same method of displaying data is also used in Figures 3–6. The meanings of the symbols in the figures are explained in the corresponding legends.

The threshold depends on the count rate, the trend of the background, as well as the trigger algorithm. Compared with the background of GRM, ECLAIRs has a larger count rate and a more rapid trend with its own combination of timescale and energy range. The top panel in Figure 2 shows that the threshold of GRM is much larger than that of ECLAIRs on the short timescale where the maximum threshold of GRM appears (e.g. on the timescale of 5 ms, the maximum threshold of GRM is 10.5 and that of ECLAIRs is 5.9); when using the long one-sided trigger algorithm on the long timescale, the threshold of ECLAIRs is very large, and its maximum threshold appears; and the long bracketed trigger obviously decreases the threshold of ECLAIRs. (E.g., in the combination of 40 s and 4–80 keV, the threshold of ECLAIRs with the long one-sided trigger algorithm is 13 and that with the long bracketed trigger is 5.) As a result, we can conclude that: (i) on the short timescale, the threshold is mainly determined by the count rate of the background and its fluctuation; and the threshold decreases as the count rate increases; (ii) on the long timescale, the threshold

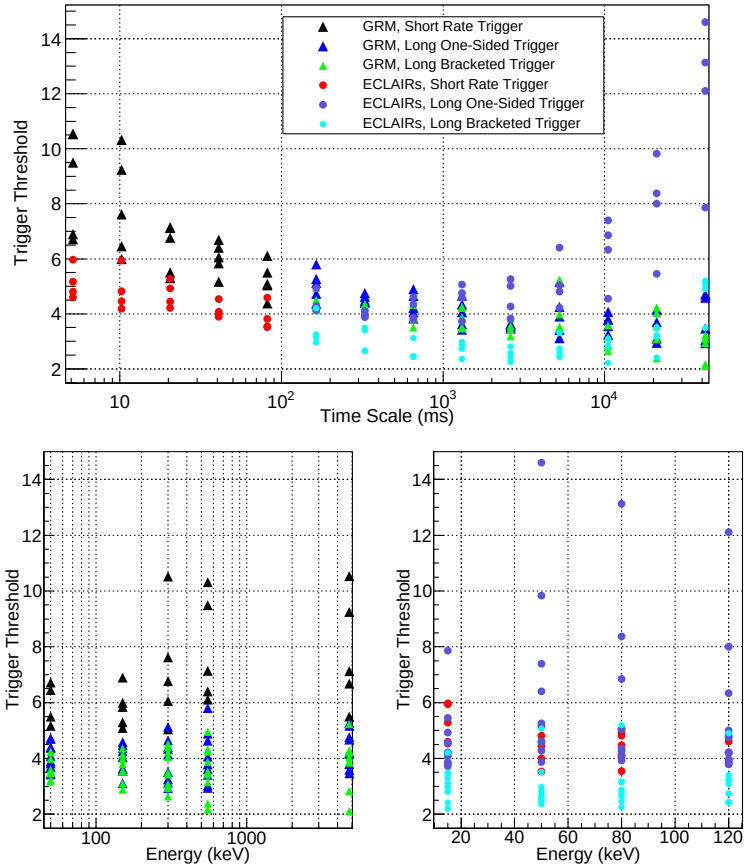

Fig. 2 The trigger thresholds ($S_{\max}$+0.5) of GRM and ECLAIRs for the different timescales (*top*) and in the different energy ranges (*bottom*). For GRM and ECLAIRs, we use the upper limit to express the corresponding trigger energy range (there is one exception: 15 keV in bottom right panel expresses the energy range 15–50 keV).

mainly depends on the trend and the algorithm; and the threshold will obviously be smaller using the long bracketed trigger than using the long one-sided trigger if the trend is rapid; (iii) on the long timescale, it is very important for ECLAIRs to adopt the long bracketed trigger algorithm to reduce the threshold to detect dark GRBs. Comparing the threshold on timescales and that for energy ranges in Figure 2, the largest threshold values of GRM lie in the energy ranges above 150 keV which is because the count rates in these energy ranges on a short timescale are the lowest. The largest threshold values of ECLAIRs lie in the energy ranges of 4–50, 4–80 and 4–120 keV because these have the most rapid trend in the background and they use a long one-sided trigger.

3.3 Trigger Efficiency

With a trigger threshold, we can compute the corresponding trigger efficiency for the set of GRBs described in Section 2 for each combination of timescale and energy range. In this section, we will use the dark GRBs which are obtained by reducing the flux of the bright GRBs by 1/10 or 1/100 while keeping other features the same. By applying the dark GRBs, the timescales and the energy

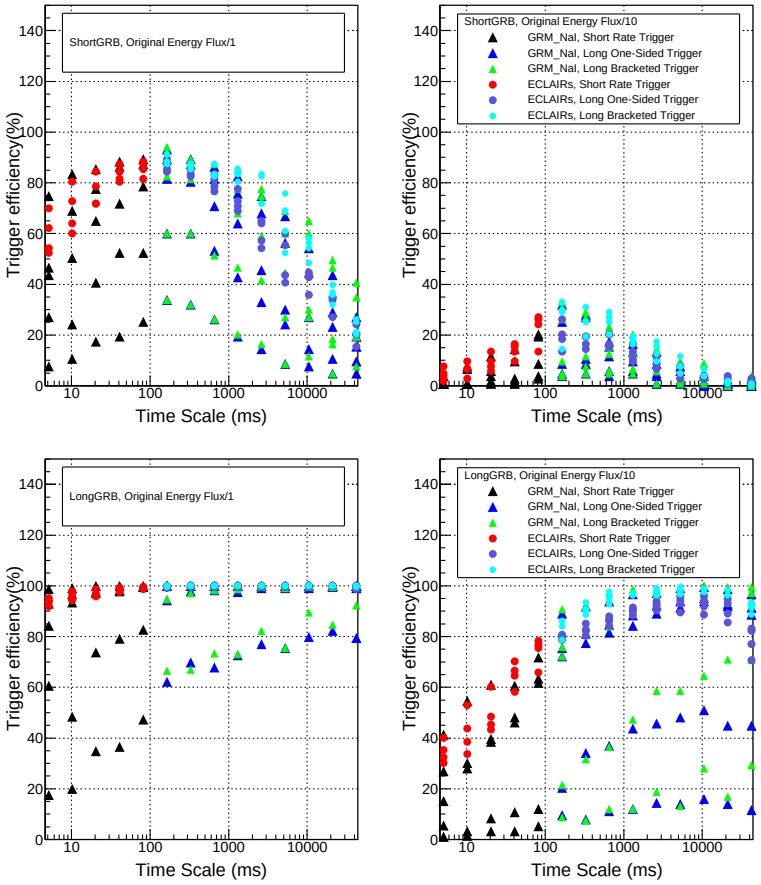

Fig. 3 *Top*: The efficiencies of GRM and ECLAIRs for bright (*left*) and dark (*right*) short GRBs on different timescales. *Bottom*: The efficiencies of GRM and ECLAIRs for bright (*left*) and dark (*right*) long GRBs on different timescales.

ranges which are most sensitive to trigger GRBs, as well as the characteristics of GRBs which are triggered in GRM and ECLAIRs, can be derived.

The variations in the trigger efficiency for short and long GRBs with different timescales are shown in Figure 3. We present the trigger efficiencies of GRM and ECLAIRs for bright GRBs in the left two panels and for dark GRBs in the right two panels. Overall, the trigger efficiency for dark GRBs is obviously lower than that for bright GRBs. In addition, Figure 3 shows that: (1) on different timescales, the maximum efficiencies of GRM and ECLAIRs are similar (e.g. on a timescale of 1 s, both the maximum efficiencies of GRM and ECLAIRs are 85.4% for bright short GRBs, and are 100% for bright long GRBs); (2) on long timescales, the efficiency with the long one-sided trigger is lower than that with the long bracketed trigger which is more obvious for ECLAIRs (e.g. on a timescale of 1 s, the maximum efficiency is 91.5% with the long one-sided trigger for the long GRBs with 1/10 of the flux of bright long GRBs, and is 96.7% with the long bracketed trigger.) because of the higher trigger threshold using the long one-sided trigger; (3) for long GRBs, GRM and ECLAIRs have higher efficiency on long timescales because the accumulation of the count rate on long timescales can increase their significance, and the efficiency on short timescales below 1 s

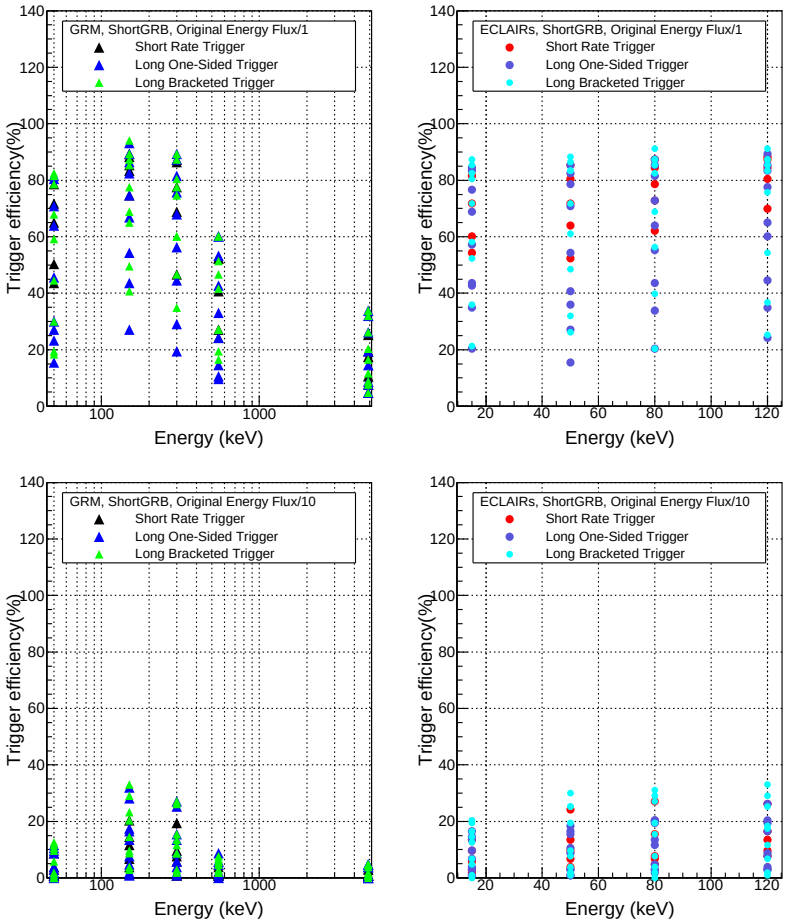

Fig. 4 The efficiencies of GRM and ECLAIRs for bright (*top*) and dark (*bottom*) short GRBs in different energy ranges.

decreases quickly as the flux of GRBs decreases; (4) for short GRBs, GRM and ECLAIRs have maximum efficiencies of a few hundred ms. (The maximum efficiencies of ECLAIRs and GRM are 89.3% and 93.2%, respectively, and both of them are on the timescale of 160 ms.)

The variations of the trigger efficiency for short and long GRBs with energy ranges are shown in Figures 4 and 5, respectively. From the maximum efficiency in each energy range, we can conclude that 50–150 keV and 150–300 keV are the most sensitive energy ranges for GRM. The efficiency for dark GRBs is obviously lower than that for bright GRBs which may be due to the narrowness of the energy ranges. Accordingly, we combine different energy ranges to form a larger one. The corresponding results are presented in Figure 6 which shows that even though the efficiency can be somewhat raised by enlarging the trigger energy range, the efficiency of dark GRBs is still much lower. The energy ranges below 300 keV are still the most sensitive. For ECLAIRs, the highest trigger efficiency for all kinds of GRBs in every energy range is very similar.

Almost all of the bright GRBs can be triggered in both GRM and ECLAIRs, especially the bright long GRBs. Therefore, we investigate the characteristics of GRBs which have triggers in GRM or ECLAIRs using dark GRBs. We extract three kinds of GRBs which have triggers only in GRM, only

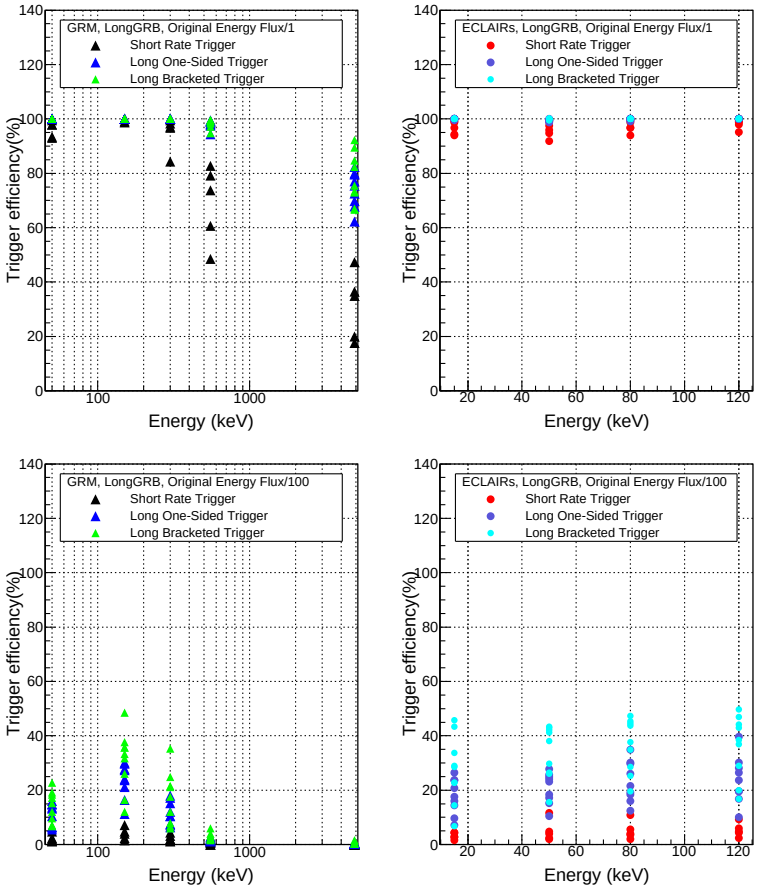

Fig. 5 The efficiencies of GRM and ECLAIRs for bright (*top*) and dark (*bottom*) long GRBs in different energy ranges.

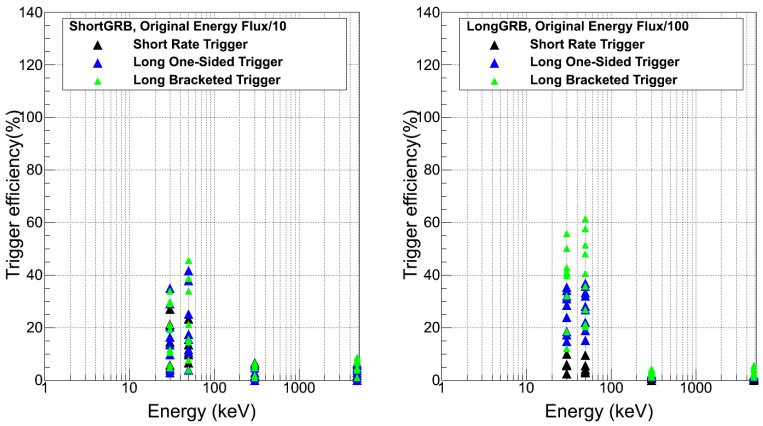

Fig. 6 The efficiencies of GRM for dark short (*left*) and dark long (*right*) GRBs in larger energy ranges (30, 50, 300 and 5000 keV indicate the energy ranges 30–150, 50–300, 300–1000 and 300–5000 keV, respectively).

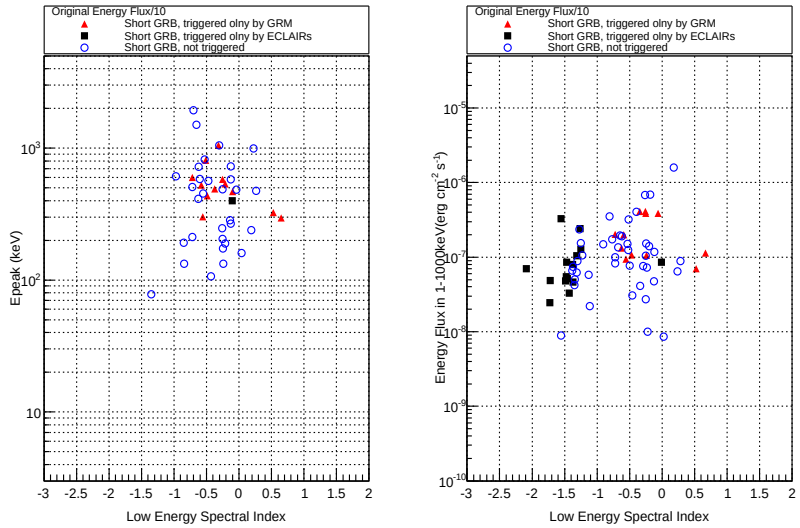

Fig. 7 The distributions of the dark short GRBs which have triggers in GRM or in ECLAIRs.

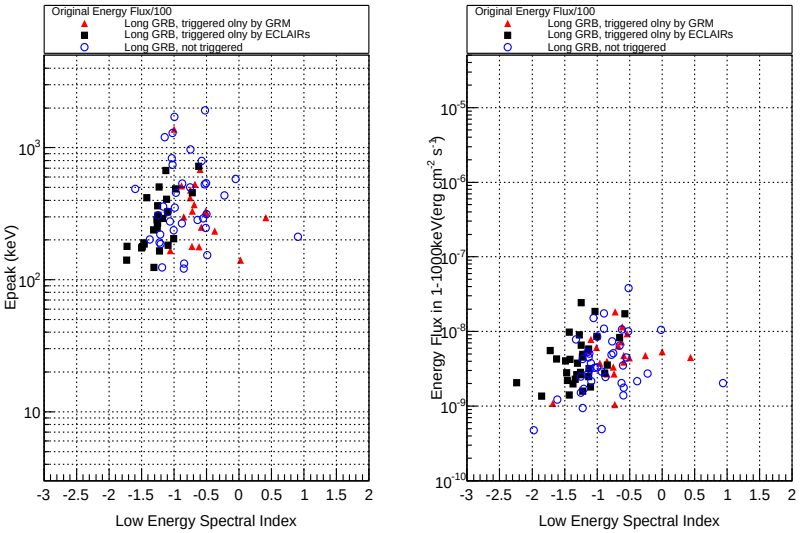

Fig. 8 The distributions of the dark long GRBs which have triggers in GRM or in ECLAIRs.

in ECLAIRs and which have triggers in neither one, respectively. We denote these three kinds of GRBs by GRM-GRBs, ECLAIRs-GRBs and NO-GRBs for convenience, respectively. The numbers of these GRBs are shown in Table 1. Their distributions on a plot of low energy spectral index vs. $E_{\rm peak}$ and low energy spectral index vs. energy flux are shown in Figures 7 and 8 in which the three kinds of GRBs are denoted by solid triangles, solid squares and hollow circles, respectively. Some of the GRBs do not have the parameter of $E_{\rm peak}$, therefore, the data in the left panels of Figures 7 and 8 are less than those in the right panels.

As the flux decreases, the characteristics of GRM-GRBs, ECLAIRs-GRBs and NO-GRBs are as follows: (1) the numbers of GRM-GRBs, ECLAIRs-GRBs and NO-GRBs gradually increase before the flux greatly decreases; (2) the low energy spectral index of GRM-GRBs is larger than that of

Table 1 The numbers of GRBs, which have triggers in GRM or ECLAIRs, when the GRBs have 1/n for the flux of the bright GRBs.

GRB Type	Trigger Type	Flux	Flux/5	Flux/10	Flux/100
Short GRB	GRM	3	9	12(0)	0
	ECLAIRs	1	9	15(14)	2
	No	5	17	42	100
	Yes	98	86	61	3
Long GRB	GRM	0	0	0	21(1)
	ECLAIRs	0	0	0	32(3)
	No	0	0	0	40
	Yes	249	249	249	209

GRM: only have triggers in GRM. ECLAIRs: only have triggers in ECLAIRs. No: neither have triggers in GRM nor in ECLAIRs. Yes: have triggers which may be in GRM or may be in ECLAIRs. The values in brackets are the numbers of GRBs with a spectrum that is modeled as a single power law.

ECLAIRs-GRBs; (3) the proportion of the GRBs with a single power-law spectrum in ECLAIRs-GRBs is much larger than that in GRM-GRBs. (2) and (3) imply that GRM is more sensitive to hard GRBs compared to ECLAIRs, and that GRM will play a very important role in measuring $E_{\rm peak}$, especially the $E_{\rm peak}$ of short GRBs.

4 THE SOLAR FLARE TRIGGERS

Solar flares (Lin 2011; Fletcher et al. 2011) are the most powerful explosions in the solar system. Out of 8021 triggers of BATSE, the fractions of GRBs and solar flares are 33.7% and 14.8%[4], respectively. There are so many triggers induced by solar flares on BATSE that it is necessary to estimate the impact of flares on GRM. SVOM will be pointed close to the anti-solar direction during a large fraction of the orbit. We can predict that the probability of the triggers caused by solar flares in GRM will be much lower than that in BATSE. BATSE can distinguish flares from GRBs mainly by location and spectrum combined with the observations of GOES (Mallozzi et al. 1993). The pointing strategy of SVOM makes ECLAIRs unable to image and localize solar flares. Thus, the ability to identify solar flares can only rely on the performance of GRM or in combination with the observations of other instruments. In this section, we will study how to distinguish the solar flares from GRBs using the data from GRM_NaI and GRM_CsI.

We use the solar flares observed by RHESSI as the sample. Discarding the events which have no position information or whose positions are zero or whose maximum energy is below 6 keV, there are a total of 57 388 solar flares that were recorded from 2002 February 12 to 2012 May 12 according to data on the website[5]. In order to estimate the impact of the flares on GRM, we need two aspects of work. Firstly, we analyze the statistical distribution of these solar flares; secondly, we perform simulations with one typical flare. Thus, we can estimate the average number of flares, which can be detected by GRM per year, and we can investigate the method to distinguish solar flares from GRBs. The distributions of the flares in the highest energy band and in the peak count per second for the energy range 12–25 keV are shown in Table 2. Most of the solar flares are soft and are not very intense. The flares having their highest energy $\geq$50 keV account for only 2.3%, and those with peak counts $\geq$400 in 12–25 keV make up 11.8%. When photons are injected from behind, the efficiency of GRM_NaI for the 100 keV photons is 0.85%, and those for the 300 keV and 800 keV photons are 4.4% and 8.5%, respectively. Accordingly, we can expect that only the solar flares with high energy and large peak counts can be detected by GRM.

[4] *ftp://umbra.nascom.nasa.gov/pub/batse/batse0/burst_trigger.lst*

[5] *http://hesperia.gsfc.nasa.gov/hessidata/dbase/*

Table 2 The distributions of the solar flares observed by RHESSI in terms of the maximum energy and the peak count for the energy range 12–25 keV.

≥E0 (keV)	N (Flare)	Proportion	≥Peak Count (count s^{-1})	N (Flare)	Proportion
12	57388	1	400	6763	0.1179
25	12550	0.21869	800	3719	0.0648
50	1333	0.02323	1000	2958	0.0515
100	221	0.00385	10000	50	0.0009
300	75	0.00131	—	—	—
800	11	0.00019	—	—	—
7000	4	0.00007	—	—	—

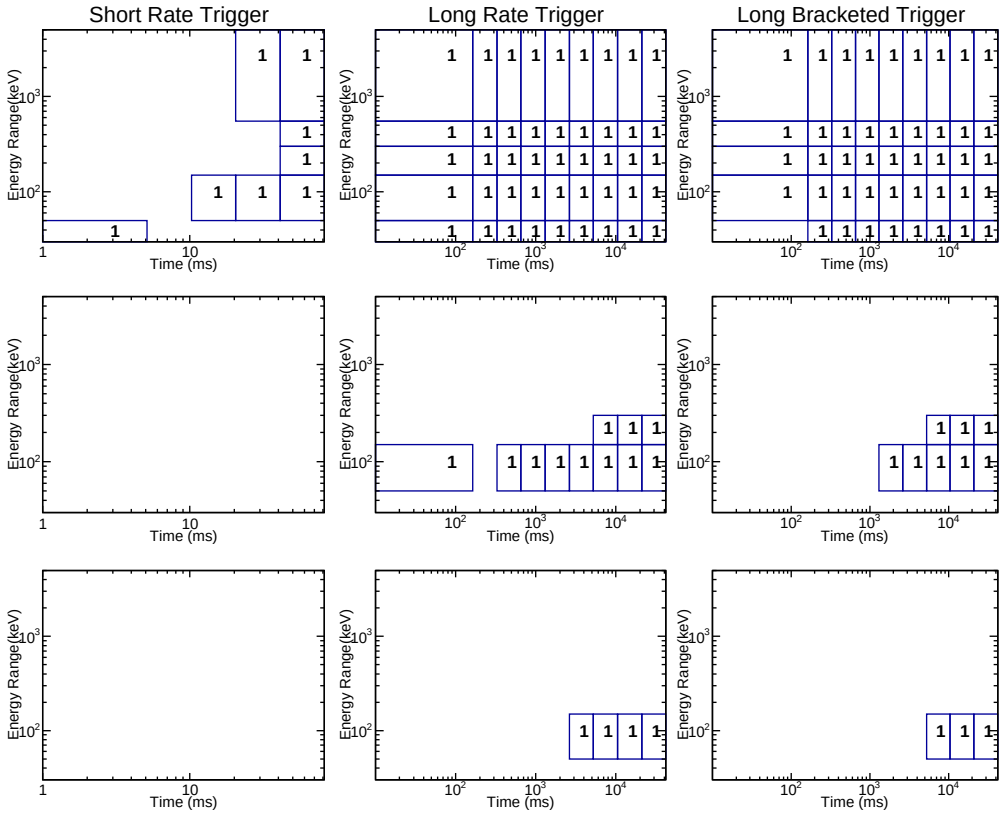

Fig. 9 The triggers of SOL2002-07-23 in GRM_NaI. From top to bottom, the corresponding classifications are X4.8, M2.4 and M1, respectively (1 in the figure means that the flare has a trigger in the corresponding energy range-timescale combination and empty means no trigger).

Solar flare SOL2002-07-23 (X4.8), whose spectrum and light curves can be found in Lin (2011) and on the website[6], is a very typical intense flare. For this flare, the measurements span almost four orders of magnitude in photon energy and more than 12 orders in flux. SOL2002-07-23 lasts about

[6] *http://hesperia.gsfc.nasa.gov/hessidata/dbase/*

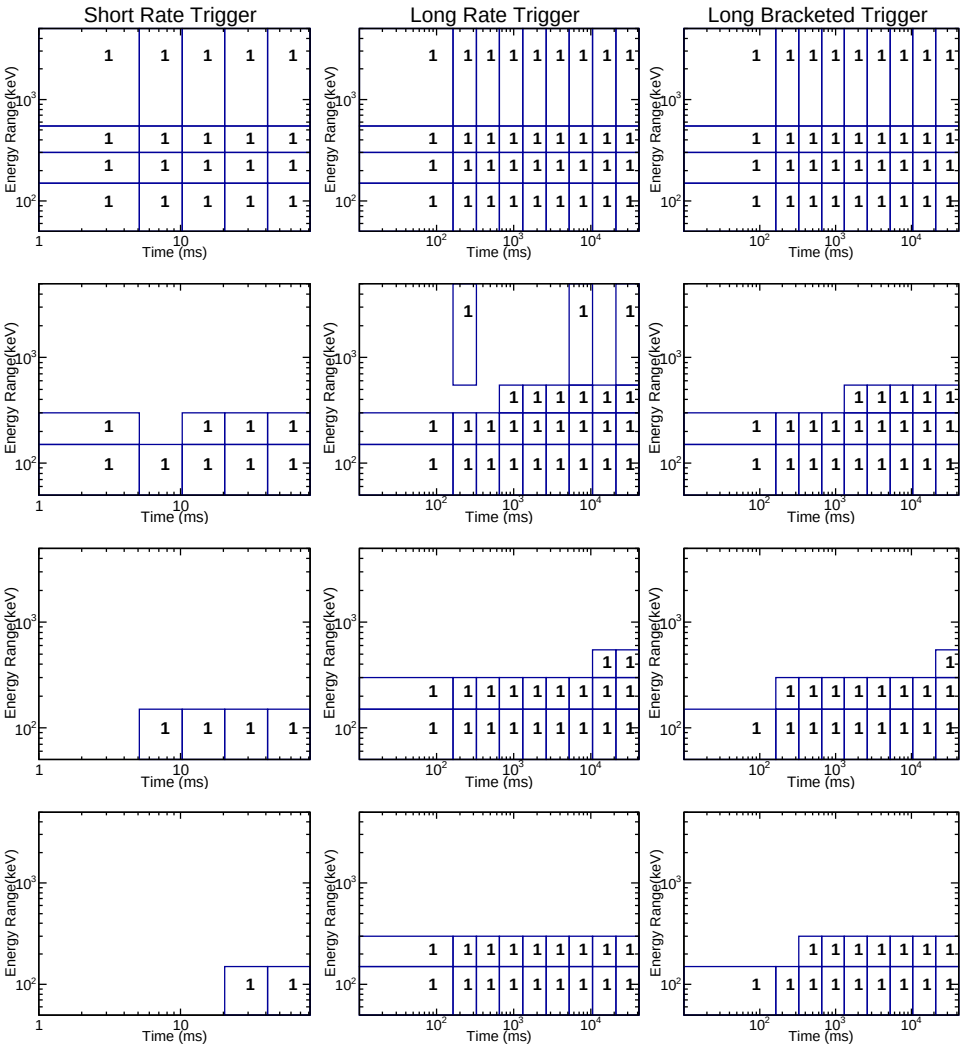

Fig. 10 The triggers of SOL2002-07-23 in GRM_CsI. From top to bottom, the corresponding classifications are X4.8, M2.4, M1 and C4.8, respectively.

one hour and its peak count in energy range 12–25 keV is about 42 341 counts s^{-1}. We assume its spectrum and light curve to be in the energy range 25–7000 keV.

Like what we did for GRBs, we decrease the flux of SOL2002-07-23 while keeping the shapes of the spectrum and light curve to obtain the flares of M2.4, M1 and C4.8. For different classifications of flares, we get the trigger results in GRM_NaI and GRM_CsI as shown in Figures 9 and 10 respectively. The X4.8 class flare triggers every energy range of GRM_NaI and GRM_CsI, though it has almost no trigger in GRM_NaI on a timescale less than 20 ms. For the M2.4 class flare, there is no trigger on short timescales; the main trigger energy range of GRM_NaI is 50–150 keV; and there are very few triggers in the energy range 150–300 keV on longer timescales ($\geq$10 s). In GRM_NaI, there is no trigger for the C4.8 class flare whose peak count is 423 counts s^{-1}. Assuming that only

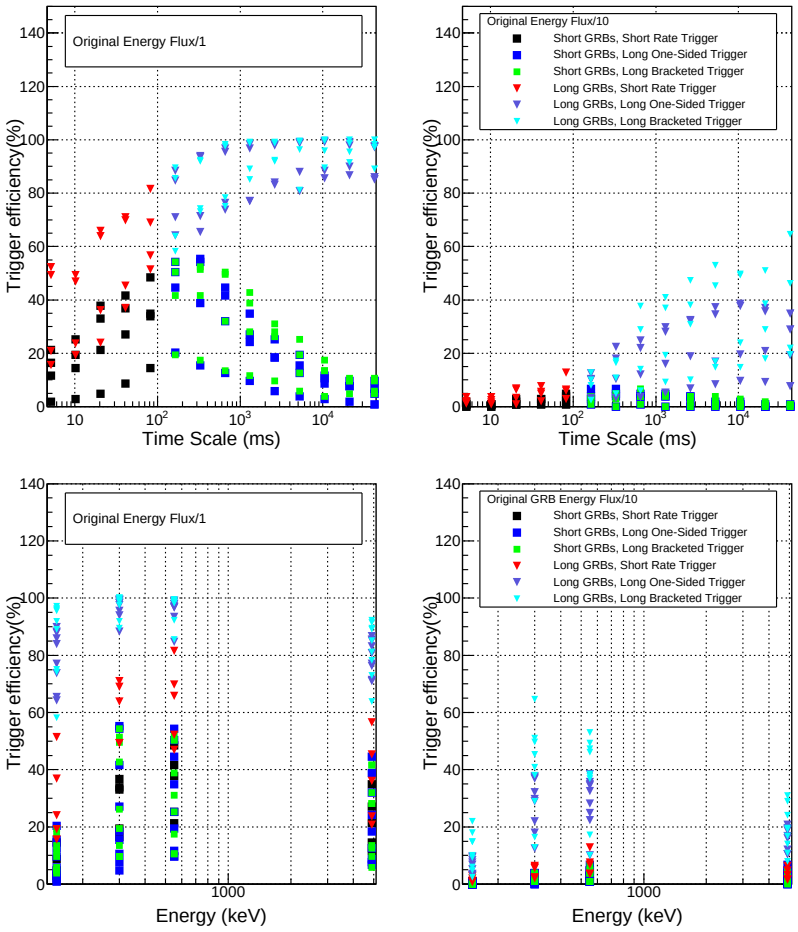

Fig. 11 The efficiencies of GRM_CsI for bright (*left*) and dark (*right*) GRBs on different timescales (*top*) and in different energy ranges (*bottom*, 150, 300, 550, and 5000 keV indicate the energy ranges 50–150, 150–300, 300–550 and 550–5000 keV, respectively).

the flares, which have energy emissions above 50 keV and peak counts more than 400 counts s^{-1}, have triggers in GRM_NaI, 187 (about 0.3%) of the solar flares observed by RHESSI will have triggers in GRM. Therefore, there are less than 20 solar flares per year which can cause false triggers in GRM_NaI.

We demonstrate the trigger efficiency of GRBs in GRM_NaI in Figures 4 and 5. Compared with solar flares, GRM_NaI is very sensitive to GRBs in the energy range 150–300 keV in addition to 50–150 keV. As shown in Figure 10, 50–150 keV and 150–300 keV are two main trigger energy ranges of GRM_CsI for solar flares, especially 50–150 keV.

Figure 11 shows that GRM_CsI is not sensitive to short GRBs (the maximum efficiency is 55.3% for bright short GRBs). The efficiency for bright long GRBs can be more than 90% on timescales larger than 160 ms. When the flux of GRBs decreases, the energy range 50–150 keV of GRM_CsI is no longer sensitive.

For GRBs, the trigger efficiency in GRM_NaI is often obviously higher than that in GRM_CsI for the same combination of energy range and timescale. For solar flares, the opposite is true. Comparing the distributions of energy ranges in which the GRBs and solar flares have triggers with relatively high efficiency, we can conclude that: (1) the sources not triggered in GRM_CsI are not likely to be solar flares; (2) the sources triggered in GRM_CsI and not triggered in GRM_NaI are not GRBs in the FOV; (3) the sources triggered outside 50–150 keV in GRM_NaI are not likely to be solar flares.

5 SUMMARY

In this work, three onboard counting rate trigger algorithms for GRM are investigated. The prime difference between the different algorithms is the method to calculate the background. They have their own advantages and disadvantages and complement each other. The short rate trigger algorithm, which is fast but has a high threshold and a rough calculation of the background, is suitable for short GRB triggers but not for dark GRB triggers. The long one-sided trigger algorithm, which can remove the trend of the background and has a lower threshold, is applicable to long GRB triggers. The long bracketed trigger algorithm, which can remove the trend of the background most accurately, has the advantage of being able to detect long GRBs, especially long dark GRBs, but it takes longer than the other two algorithms. We can use them simultaneously in order to increase trigger efficiency and to detect GRBs as early as possible. The computations of trigger efficiency based on the given GRB sample show that 50–150 keV and 150–300 keV are the most sensitive trigger energy ranges for GRM and that a few seconds and several hundred milliseconds are the timescales for sensitivity to long GRBs and short GRBs, respectively. We applied the same trigger algorithms to ECLAIRs, and investigated the trigger characteristics of GRM and ECLAIRs. In addition, we find that the solar flares can be distinguished from GRBs by analyzing the distribution of triggers in energy ranges of GRM_NaI and GRM_CsI. Less than 20 solar flares per year, on average, can cause triggers in GRM_NaI according to the statistics of the solar flares observed by RHESSI from 2002 to 2012 and the simulations using the typical SOL2002-07-23.

We used a simplification during the simulations. We keep the GRBs in the center of the FOV and keep the photons perpendicular to the detector plane which is an ideal case. With this simplification, the detection efficiency of the instruments is usually the highest which might make the trigger efficiency higher than what it needs to be. The investigation with GRBs in various positions in the FOV needs further work.

According to the observations of BATSE, fluctuations in discrete sources, soft gamma repeaters (SGRs) and magnetospheric events, which are mainly the electron precipitation events (Mallozzi et al. 1993), can also cause many triggers. The triggers that appeared as a transient source emerging from behind the Earth can be easily classified since they follow a pattern of occultation at predictable times. The SGRs can be identified primarily by their soft spectra and typical short durations (about 0.1 s) (Mallozzi et al. 1993; Kouveliotou et al. 1992). However, the key to identifying the triggers by their electron precipitation events and the source flares is the localization ability of the instrument based on the experiences of BATSE (Horack et al. 1991; Meegan et al. 1993). GRM consists of two identical detectors which point to the same direction, but has no localization ability. By contrast, ECLAIRs has image and localization abilities. Accordingly, GRM can identify the GRB triggers and reject the false triggers more effectively by taking full advantage of the trigger information from ECLAIRs. Therefore, the investigation of the simultaneous operation of GRM and ECLAIRs for GRB triggers is another important task to which we will pursue in future studies based on the work described in this paper.

Acknowledgements The work was supported by the National Basic Research Program of China (973 Program, 2009CB824800), the National Natural Science Foundation of China (Grant No. 10978001) and the Knowledge Innovation Program of the Chinese Academy of Sciences (Grant No. 200931111192010).

References

Basa, S., Wei, J., Paul, J., Zhang, S. N., & Svom Collaboration, 2008, in SF2A-2008, eds. C. Charbonnel, F. Combes, & R. Samadi, 161
Dong, Y.-W., Wu, B.-B. et al., 2009, Science in China G: Physics and Astronomy, 52, 1
Fenimore, E. E., & Galassi, M. 2001, in Gamma-ray Bursts in the Afterglow Era, eds. E. Costa, F. Frontera, & J. Hjorth, 393
Fenimore, E. E., McLean, K., Palmer, D., et al. 2004, Baltic Astronomy, 13, 301
Fenimore, E. E., Palmer, D., Galassi, M., et al. 2003, in Gamma-Ray Burst and Afterglow Astronomy 2001: A Workshop Celebrating the First Year of the HETE Mission, American Institute of Physics Conference Series, 662, eds. G. R. Ricker, & R. K. Vanderspek, 491
Fletcher, L., Dennis, B. R., Hudson, H. S., et al. 2011, Space Sci. Rev., 159, 19
Ghirlanda, G., Celotti, A., & Ghisellini, G. 2002, A&A, 393, 409
Ghirlanda, G., Ghisellini, G., & Celotti, A. 2004, A&A, 422, L55
Godet, O., Sizun, P., Barret, D., et al. 2009, Nuclear Instruments and Methods in Physics Research A, 603, 365
Horack, J. M., Fishman, G. J., Meegan, C. A., Wilson, R. B., & Paciesas, W. S. 1991, in American Institute of Physics Conference Series, 265, 373
Kaneko, Y., Preece, R. D., Briggs, M. S., et al. 2006, ApJS, 166, 298
Kouveliotou, C., Norris, J. P., Wood, K. S., et al. 1992, ApJ, 392, 179
Lin, R. P. 2011, Space Sci. Rev., 159, 421
Mallozzi, R. S., Paciesas, W. S., Meegan, C. A., Fishman, G. J., & Wilson, R. B. 1993, in American Institute of Physics Conference Series, 280, eds. M. Friedlander, N. Gehrels, & D. J. Macomb, 1122
Mandrou, P., Schanne, S., Cordier, B., et al. 2008, in American Institute of Physics Conference Series, 1065, eds. Y.-F. Huang, Z.-G. Dai, & B. Zhang, 338
McLean, K. M., Fenimore, E. E., Palmer, D., et al. 2004, in Gamma-Ray Bursts: 30 Years of Discovery, American Institute of Physics Conference Series, 727, eds. E. Fenimore, & M. Galassi (Melville:AIP), 667
Meegan, C., Fishman, G., Wilson, R., & Paciesas, W. 1993, in American Institute of Physics Conference Series, 280, eds. M. Friedlander, N. Gehrels, & D. J. Macomb, 1117
Nava, L., Ghirlanda, G., Ghisellini, G., & Celotti, A. 2011, A&A, 530, A21
Paul, J., Wei, J., Basa, S., & Zhang, S.-N. 2011, Comptes Rendus Physique, 12, 298
Schanne, S., Cordier, B., Götz, D., et al. 2008, in International Cosmic Ray Conference, 3, 1147
Tavenner, T., Fenimore, E., Galassi, M., et al. 2003, in Gamma-Ray Burst and Afterglow Astronomy 2001: A Workshop Celebrating the First Year of the HETE Mission, American Institute of Physics Conference Series, 662, eds. G. R. Ricker, & R. K. Vanderspek, 97
Zhao, D., Cordier, B., Sizun, P., et al. 2012, Experimental Astronomy, 34, 705